Collaborative Vision-Based Precision Monitoring of Tiny Eel Larvae in a Water Tank

JUHWAN KIM[1], (Member, IEEE), **SEOKYONG SONG**[1], **TAESIK KIM**[1], **YOUNG-WOON SONG**[1], **SHIN-KWON KIM**[2], **BAE-IK LEE**[2], **YONGWOON RYU**[2], AND **SON-CHEOL YU**[3], (Member, IEEE)

[1]Department of Convergence IT Engineering, Pohang University of Science and Technology, Pohang-si 37673, South Korea
[2]Aquaculture Research Division, National Institute of Fisheries Science (NIFS), Busan 46083, South Korea
[3]Division of Advanced Nuclear Engineering, Pohang University of Science and Technology, Pohang-si 37673, South Korea

Corresponding author: Son-Cheol Yu (sncyu@postech.ac.kr)

ABSTRACT This paper proposes a novel monitoring system in which two cameras installed outside the water tank collaborate to photograph eel larvae for tracking and analysis. Long-term and periodic observations of fish can provide important information about their life. However, fresh eel larvae have a tiny and transparent body, making it difficult to observe and track them through optical vision. To address this problem, we proposed a monitoring system that uses a fixed high-resolution camera to observe the entire breeding tank and a telecentric zoom camera on a Cartesian robot to track and observe a single larva. In addition, the collaborative vision-based object search method helps the zoom camera to capture photographs of the tiny larvae. We verified the method by placing several 3D plastic models similar to eel larvae in the water tank at predetermined locations. We then conducted an experiment using actual larvae and were able to obtain videos of the larvae. Subsequently, we analyzed the videos to obtain the population estimation, shape, and size of the larvae. As a result, we established a novel eel larva monitoring system and conducted actual larva-monitoring experiments.

INDEX TERMS Eel larvae, aquaculture, 3-D tracking, fish tracking, animal behavior, motion trajectory.

I. INTRODUCTION

Observing the ecology of fish in the sea is extremely difficult because of the environment. It is almost impossible to track individual fishes in the vast sea. Furthermore, deep seas are inaccessible due to the high water pressure. In addition, fast moving fishes are even more difficult to be photographed. Therefore, most underwater biological imaging is performed for a specific area rather than for a specific fish; as a result, only the investigation and analysis of an observed fish can be performed [1]. In particular, it becomes more challenging to observe the ecology of the larvae hatched from eggs, rather than large adult fish. Wild eel eggs were first discovered in 2009 [2]. Until then, there had been only speculation about spawning sites, and their exact location and time of spawning were not known in detail [3].

Due to climate change, fishery movements, and microplastics, aquaculture businesses that produce farmed fishes are growing. With the development of aquaculture technology,

The associate editor coordinating the review of this manuscript and approving it for publication was Charith Abhayaratne.

it is possible to facilitate the necessary requirements for a single fish in artificial water tanks located on land, enabling facile observation and analysis of live fish. In particular, in the case of fresh eels, which have actively undergone complete aquaculture research in recent years, larvae hatched from eggs grow to become leptocephalus, grow further into grass eels, and then grow into adult eels [4]. This breeding process is different from that of ordinary fish, and detailed observations of the larval life cycle can play a significant role in understanding eels' lives.

In the field of modern aquaculture technology, fish life-specific feeds, breeding water filtration devices, and aquaculture methods are being actively researched [5]. Many studies have been conducted on intelligence and automation using mechanized aquaculture systems [6]. Modern aquaculture aims to minimize human resources and achieve efficient large-scale aquaculture system for industry, and many recently built farms have automated feeding and management systems [7], [8]. In particular, for the larval stage, researchers have automated the water tank's feeding and cleaning processes. This automation research is valuable

because it automates the work currently performed by manual labor. However, for more effective breeding, a technology is required that can be used for automated breeding by monitoring and analyzing the environment and monitoring the fishes.

Breeding environment monitoring involves the accumulation of data obtained by measuring the temperature, humidity, and dissolved oxygen in the breeding water with sensors [9]. Moreover, by directly observing the object, researchers can determine the object's size and condition via a sampling process [10]. However, if the tiny larvae were observed by sampling, only their static appearance could be observed because the sampled larvae were dead. This also results in the loss of larvae due to the sampling process, and the observation period is relatively long. Therefore, if it is possible to perform direct observation within the water tank where breeding takes place, imaging can be performed at any time for observation in a short period, and we can obtain additional information, such as the movements in the water tank.

Many researchers have proposed photographing zebrafish directly in water tanks [11]–[15]. They modeled the fish's behavior to analyze the movement and suggested a solution when two fish overlapped in an image. Thereafter, a system for tracking and observing behavior in 3-D is proposed [16], [17]. A study using zebrafish as neurobehavioral research has also been proposed [18]. Many studies have been conducted on cucumbers, an aquatic organism with a relatively slow speed and a unique body [19]–[21]. Along with the detection of sea cucumbers using vision technology, observational studies in the sea and a water tank have been proposed [22], [23]. However, previous research results can be observed by the far-view camera outside the water tank because they used relatively large fish.

In the case of zebrafish, larval monitoring studies have been conducted. In most studies, larvae were transferred to a dish, rather than to a water tank for monitoring and imaging [24]–[28]. Using a high-resolution camera, a zebrafish larva was placed on a 2-D plane, and trajectory was extracted through various photographs, and the behavior was analyzed. However, it was challenging to shoot in a water tank for breeding and to expand it to 3-D. Through larval monitoring, we can obtain the necessary information. Monitoring data can be used in various ways in the field of model organism research [29], and the results obtained through fluorescent staining can capture the appearance of internal organs [30]. In addition, in the fully enlarged and still image of the larva, the heart's position can be detected [31]. These data were obtained by sampling and fixing the larvae to an imaging device and observing it. If long-term observations can be performed in a living state, more meaningful results can be obtained in the future.

In this study, we developed a collaborative vision-based precision monitoring system equipped with a fixed high-resolution camera that records the entire water tank of eel larvae and a telecentric zoom tracking camera that accurately moves in three axes and can track and photograph the small larvae. In addition, we propose a practical photographing and analysis method. We analyzed the fixed high-resolution camera image to detect the larvae in the water tank, and then proposed a collaborative algorithm that allows the tracking zoom camera to capture the larvae by finding the larvae's high-density area. We conducted a demonstrative model experiment by randomly placing plastic models of small eel larvae in a water tank. In the experiment, we confirmed that tiny larvae can be successfully observed using our method. Furthermore, the telecentric zoom camera was able to find and track the actual eel larvae placed in the tank for effective imaging. Subsequently, we extracted quantitative values from the larvae images using the shape of the body analysis. As a result, we successfully photographed eel larvae based on the two collaborative cameras, and the quantitative values analyzed from the videos could be used as an evaluation index for larval eel farming.

The contribution of this paper lies in the following aspects:

1) A monitoring system for tiny eel larvae that was designed for real-time observation and analysis outside the water tank for aquaculture was developed.
2) Collaborative vision-based tiny object search method helps the zoom camera shoot tiny larvae.
3) Video shooting, population estimation, trajectory extraction, and body length measurement were performed through experiments of larva models and actual eel larvae.

The remainder of this paper is organized as follows. Section 2 explains the proposed monitoring system design in detail, collaborative tiny larvae shooting methods and image-analysis methods for breeding management. In Section 3, we describe the experiments using the eel larva models for quantitative evaluation. In Section 4, we present the experimental results with actual eel larvae to evaluate the proposed methods. Finally, the conclusions are given in Section 5.

II. MATERIALS AND METHODS
A. AUTOMATED EEL LARVAE AQUACULTURE
The eel to be observed is *Anguilla japonica*. Recently, many researchers have conducted breeding experiments on the hatching of the larvae of this fish. Long-term breeding of eel larvae is a monotonous task. Essentially, it is necessary to feed the larvae, clean the water tank, and control the seawater supply. We have developed an automated breeding system that performs these functions using a robotic arm and includes a breeding water control system using a fine control valve, as shown in Fig. 1.

We used a robot servomotor and a linear rail motor to position the endpoint for feeding and cleaning the tank to the desired location. All frame structures are made of 3D-printed plastic, aluminum, and stainless steel so that they are hygienic and do not affect the larvae. As a result, we mounted a 15-cm-long tip that was easy to clean and could supply the desired amount of food to the desired location through a metering pump. In addition, because the long tip connects the
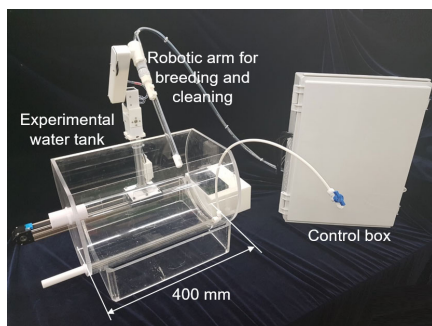
FIGURE 1. Automated aquaculture system for eel larvae.

pipe through a valve, water can be discharged, and the water tank can be cleaned with constant water pressure. We controlled the flow rate according to the flow meter's value by connecting the high-resolution servo to the fluid control valve. This device can accurately control the flow rate in units of 0.1 L/min or less and control the flow rate supplied to the water tank, as well as the cleaning flow rate. The entire system was controlled wirelessly using a central control computer. Many automated breeding systems can individually perform feeding and tank cleaning at the desired cycle time. We can adjust the amount of food or flow and schedule all the feeding and cleaning tasks for a set time.

We confirmed that eel larvae can be reared only with an automated system through several breeding experiments without manual labor. Thus, we showed that automated eel larvae aquaculture could be formed. After we completed the system, we were required to understand the optimal breeding method by controlling various breeding parameters. To control these parameters, it is essential to recognize the current breeding status by observing the larvae in the water tank to control the various parameters. Therefore, we attempted to develop a monitoring system that can obtain data for breeding management through observations.

B. BREEDING MONITORING SYSTEM FOR AUTOMATED AQUACULTURE

The aquaculture of living organisms must lead to significant rearing results in a suitable feed and environment, producing and hatching eggs. The larvae hatched from the egg grow to become a child, which is the stage before becoming an adult. This growth occurs in a small tank and food is fed into the circulating water. Long-term breeding is necessary for the growth of the hatched larvae. We divided the control group and the experimental group, and repeated the breeding experiment to find a breeding environment for a healthy and high survival rate. We observed all repeated breeding experiments manually by directly counting the number of larvae over time and comparing the survival rate over a certain period. However, because the experiment deals with the entire organisms, breeding experiments frequently fail for unknown reasons, and it is challenging to frequently but inaccurately count the size of the larvae directly. In addition, a one-variable experiment that compared the number of larvae weakened the efficiency of long-term breeding experiments. Therefore,
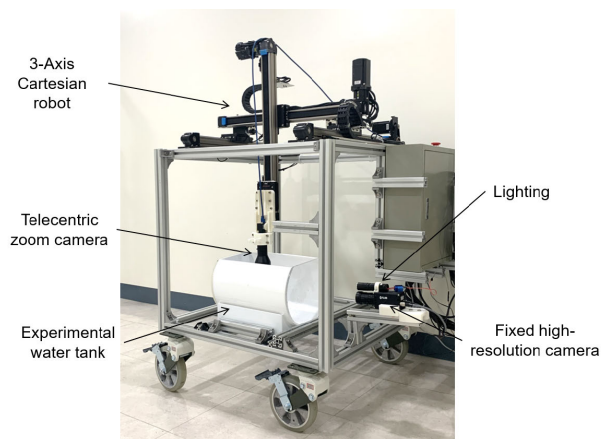

FIGURE 2. Overview of the vision-based precision monitoring system.

through photography and analysis, the number counting of the larvae can be measured in a more detailed time unit, and we can add a quantitative variable for the detailed motion of the larvae. As a result, practical eel larval breeding experiments can be conducted.

We selected two factors to measure larval breeding. The first was the number of larvae counted via image processing. A camera was used to capture the entire breeding tank. Because counting can be performed frequently at regular time intervals, we can conduct a more detailed larval survival analysis. In particular, because the point at which the number of larvae decreases is that at which the larvae die, it can be used to analyze the cause of larval death.

The second factor was the detailed observation of a single larva and the quantitative analysis of the same. The information obtained by magnifying and observing the larvae of less than 10 mm is the shape and motion according to continuous images. In terms of the larva's appearance, we can observe the extent of its physical growth. Here, we can determine the approximate volume, including the length of the larva. If it is possible to recognize and classify the larva's appearance, then determining whether the larva is damaged is also possible. Thereafter, we examined the activity of the larvae. The larva's activity quantifies the movement, which in turn enables the measurement of the larva's swimming ability.

C. MONITORING SYSTEM DESIGN

We designed a collaborative camera to capture the larvae, as shown in Fig. 2. After the eggs hatched, the larvae were 10 mm or less, and breeding began in the small water tank. The tank was made of white acrylic, except for the side on which the fixed high-resolution camera was mounted to keep the camera shooting background constant. A constant background is an essential part of observing tiny larvae because the larvae have transparent bodies, and their appearance is strongly influenced by the background. Therefore, a white background facilitates better recognition and observation. The tank was cylindrical and the top was cut off. The entire frame was made of an aluminum profile, and the wheels were attached to facilitate movement. The tank was fixed in the
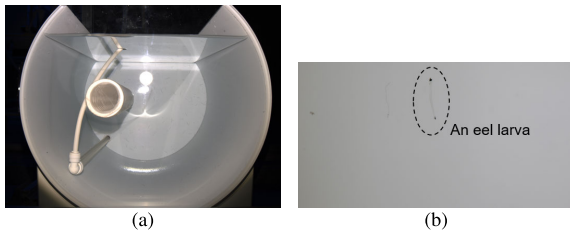
FIGURE 3. Example output images. (a) Fixed high-resolution camera image and (b) telecenric zoom tracking camera image.

correct position to perform tank shooting under the same conditions. Further, we installed a telecentric zoom tracking camera and fixed high-resolution camera on the bare frame, which we attached to a Cartesian robot that could move in three axial directions [32].

1) LIGHTING UNIT

Lighting is an essential element for capturing images. Because the area of focus changes depending on the aperture, increasing the brightness to the extent possible provides a broad focus area. Because the water tank size is fixed in integrating the monitoring system, the lighting suitable for the size of the water tank must have a constant brightness. Thus, we installed the lighting unit by mounting an LED in the same direction for a fixed camera and set up the lighting to form a uniform ambient light. The lighting unit was controlled by an electronic switch and turned on only during shooting to avoid affecting the larvae. The actual filming takes approximately 30 s, and because the filming takes place in a long cycle, the impact on the life of larvae is minimal.

2) FIXED HIGH-RESOLUTION CAMERA

A fixed high-resolution camera was used to obtain specific information by capturing the entire tank. Therefore, information on several small eel larvae can be obtained to the extent possible for obtaining high-resolution images. The camera was equipped with a 1/1'' CMOS sensor, and it can shoot high-resolution images at 60 FPS with a 10 GigE interface. A 12-mm fixed focus lens was attached, wide enough to be focused inside the tank. The camera was centered in the cylindrical water tank and fixed to the aluminum profile at a distance that can be entirely focused. Fig. 3 (a) shows a fixed high-resolution camera image.

3) TELECENTRIC ZOOM TRACKING CAMERA

A telecentric zoom tracking camera was used to zoom in on a single larva. The larva is difficult to observe in detail because it moves in a tank with a small size of less than 10 mm. Therefore, we used a camera with a zoom lens to obtain an enlarged image at a close distance, tracking the larva with physical movement.

The camera is equipped with a 1'' CMOS sensor, and it can shoot high-resolution images with a USB 3.1 interface at 42 FPS. This camera has a telecentric lens with a PMAG of 0.367×, a depth of field of 4 mm, and a working distance of 169 mm. This lens can obtain an image with a sense of
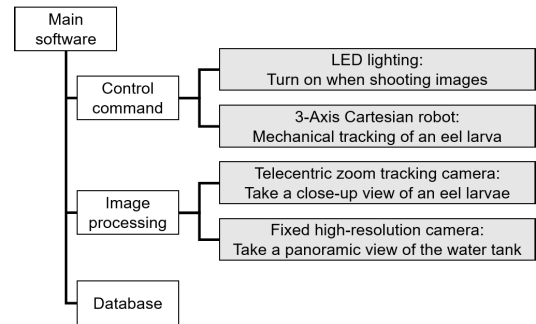

FIGURE 4. Configuration of the proposed monitoring system.

perspective removed, so it is possible to measure the larva's size and volume using only the captured image [33]. Further, because the area to be focused on is accurately fixed, knowing the location of the camera can accurately determine the location of the captured larva. In other words, if the larva is tracked and observed with an appropriate focal point as the center, the camera's movement path and the movement path of the larva match. Fig. 3 (b) shows an image from the telecentric zoom tracking camera.

This telecentric zoom tracking camera is attached to a Cartesian robot that can move in three axes (0.1 mm) to realize physical tracking. Because this robot minimizes vibration and can move the camera to the desired position, it is easy to find the larva by moving the camera's working field. The camera shoots while looking down from the top of the tank. However, owing to the limitation of its short focal area, it is only possible to image the larvae in some areas, not the entire tank.

4) CONFIGURATION OF THE MONITORING SYSTEM

In the monitoring system, each camera performs an independent imaging. However, an integrated operating system, such as that shown in Fig. 4, is required to simultaneously monitor both cameras and use far-field images when performing zoom camera tracking. We constructed a single-board computer with a 10 GigE receiving card and a USB 3.1, to acquire images from both cameras in real time. In addition, we built a software system to control the LED operation and a 3-axis Cartesian robot through RS232 communication. We then stored the information obtained from the video in a database inside the computer. As a result, we recorded all the information extracted from the aquaculture breeding works and the image processing results with the timetable.

D. COLLABORATIVE VISION-BASED TINY OBJECT SEARCH METHOD

Observing the eel larva using a telecentric zoom tracking camera requires image processing that is fused with a fixed high-resolution camera. Because the zoom camera has a very narrow field of view, the eel larva must be recognized in the focal area to start tracking. For this, the process of searching for an eel larva by moving the camera with a 3-axis Cartesian robot. However, there is a limit in identifying a tiny eel larva in a relatively large tank via a random search. Therefore,
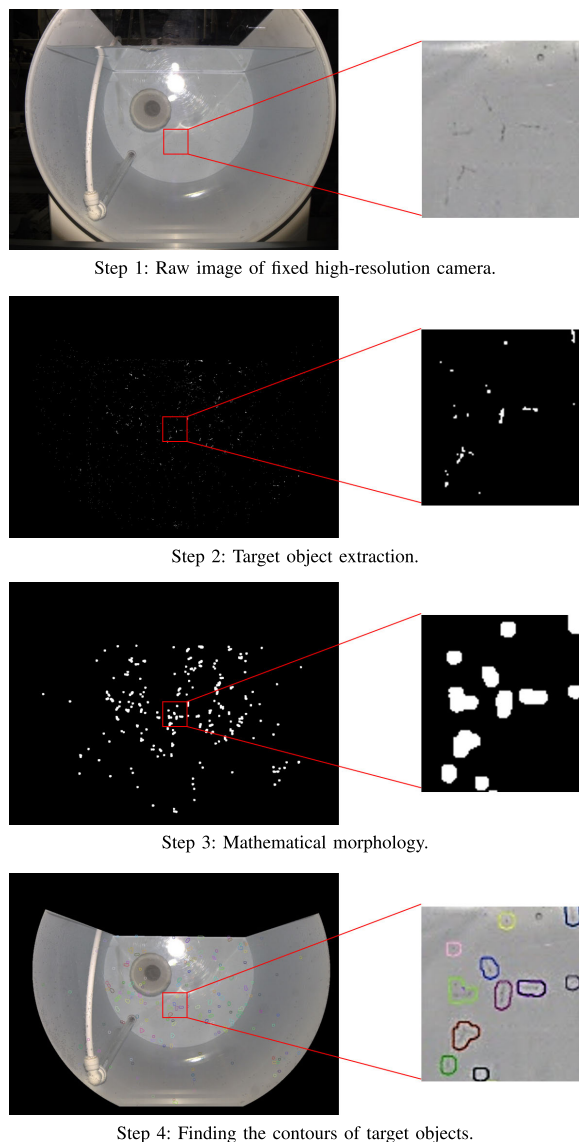
Step 1: Raw image of fixed high-resolution camera.

Step 2: Target object extraction.

Step 3: Mathematical morphology.

Step 4: Finding the contours of target objects.

FIGURE 5. Image-processing procedure for initial larvae scan.

we implemented a camera fusion-based capturing method that recognizes the location of a high density of eel larvae using a fixed high-resolution camera and performed a search around this location.

1) INITIAL SCAN OF TARGET OBJECTS, LARVAE

There are several ways to scan an object in a water tank. In general, we can use an object-detection algorithm for a shape to be found in an image. However, most methods are slow and cannot perform real-time processing or require high computer performance. Moreover, the initial larval scan is a preprocessing process used to find the searching path. Therefore, because we have completely fixed the positions of the camera and the water tank, we performed an initial larval scan using a simple image-processing technique. Foreground subtraction is an algorithm that identifies moving objects in images. However, if the water quality is not clear and there are many impurities, moving objects may be
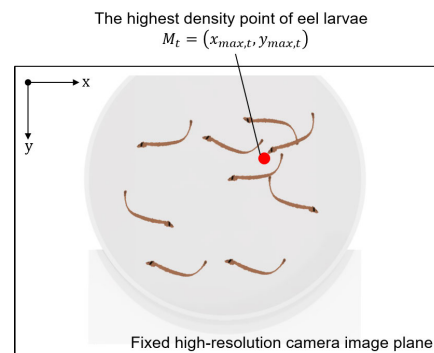

FIGURE 6. Example of the highest density point of eel larvae.

incorrectly recognized. However, because we monitored the water tank where aquaculture was taking place, the filtered seawater was continuously supplied, and the water quality was clear. In addition, impurities other than live eels were collected on the drain side and removed by periodic water bath cleaning. Therefore, the only moving objects in the fixed high-resolution camera image, which can identify a moving object and recognize each bundle of pixels as a larva, are the larvae.

We describe the overall image-processing steps for larval recognition in Fig. 5. First, we masked the active areas used in the images and then cropped an area for image processing using a filter prepared in advance. Second, we extracted the foreground mask using an algorithm based on the Gaussian mixture model [34]. Third, we removed the noise through a series of mathematical morphology processes, such as erosion and dilation, on the foreground mask result. Finally, outline extraction was performed to find more than an individual pixel's contours and recognize the pixel as a larva.

The evaluation of the scan result can be indirectly verified through the trend according to the number of eel larvae. We recorded videos from 0 to 500 larvae in increments of 20. The result of foreground subtraction on each image exhibits a trend in Eq. (17), as shown in Fig. 15. As a result, we can agree that the larvae scan result has a valid value.

$$R_{i,t} = \{(x, y) \in I_t | \text{foreground subtraction}\}. \quad (1)$$

where $R_{i,t}$ is the estimated eel larva region, I_t is the tth frame image, $i = \{1, 2, \cdots, N_t\}$, and N_t is the estimated number of eel larvae at the tth frame.

$$CM(R_{i,t}) = X_{i,t} \quad (2)$$

where CM is the center of mass in the contour region and $X_{i,t}$ denotes the ith eel larva's coordinate vector on the tth fixed high-resolution camera image plane.

2) SEARCHING PATH OF TELECENTRIC ZOOM TRACKING CAMERA

We can find the coordinates of the highest larvae density by using the kernel density estimation method from the recognized larvae of the fixed high-resolution camera image [35]. Given that the measured $X_{i,t} = \{x_{i,t}, y_{i,t}\}$ is obtained from a
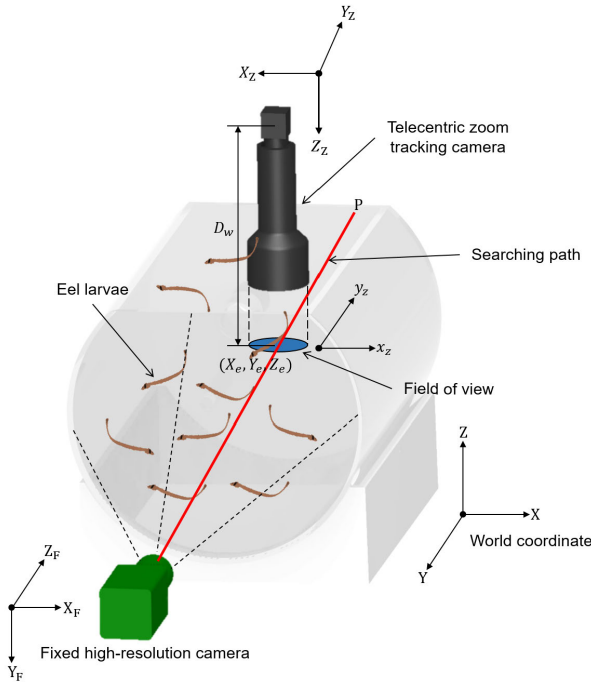
FIGURE 7. Coordinates of the cameras.

distribution with the density function $f_H(X_t)$, we can calculate the kernel density estimate at X_t as

$$\hat{f}_H(X_t) = \frac{1}{N_t} \sum_{i=1}^{N_t} K_H(X_t - X_{i,t}) \tag{3}$$

where H is the smoothing 2×2 matrix and K is the kernel function. If we choose the kernel function as the standard multivariate normal kernel, we can obtain K_H as follows:

$$K_H(X_t) = \frac{2\pi}{|H|} exp\left(-\frac{1}{2}X_t^T H^{-1} X_t\right) \tag{4}$$

where H denotes the covariance matrix. Then, we can obtain the maximum value of the density function $f_H(X_t)$, which can be called $M_t = \{x_{\max,t}, y_{\max,t}\}$.

$$M_t = \arg \max (f_H(X_t)) \tag{5}$$

Next, we can obtain the path corresponding to the M_t point so that the field of view of the zoom camera can perform searching. This path is a straight line projected from the camera sensor to M_t. Because M_t is a pixel image coordinate, it must be converted to world coordinates to obtain a functional equation. However, we must first convert it into camera coordinates. For the M_t coordinates $\{x_{\max,t}, y_{\max,t}\}$, we modeled the relationship between the 3D coordinates of the camera coordinates by homography, as follows:

$$s \begin{bmatrix} x_{\max,t} \\ y_{\max,t} \\ 1 \end{bmatrix} = K_{\text{fixed}} T_{pers}(1) \begin{bmatrix} X_{\text{fixed}} \\ Y_{\text{fixed}} \\ Z_{\text{fixed}} \\ 1 \end{bmatrix} \tag{6}$$

$$K_{\text{fixed}} = \begin{bmatrix} f_x^{\text{fixed}} & 0 & c_x^{\text{fixed}} \\ 0 & f_y^{\text{fixed}} & c_y^{\text{fixed}} \\ 0 & 0 & 1 \end{bmatrix}. \tag{7}$$

$$T_{pers}(1) = \begin{bmatrix} 1 & 0 & 0 & 0 \\ 0 & 1 & 0 & 0 \\ 0 & 0 & 1 & 0 \end{bmatrix} \tag{8}$$

Here, s is an arbitrary constant other than 0, K_{fixed} is the intrinsic parameter of the fixed camera, and $T_{pers}(1)$ is the projection transformation matrix of the normalized image plane. f_x^{fixed} and f_y^{fixed} are the focal lengths of the fixed camera, and c_x^{fixed} and c_y^{fixed} are the principal points.

Next, when the position of the fixed camera in the world coordinate is $(F_x^{\text{fixed}}, F_y^{\text{fixed}}, F_z^{\text{fixed}})$ and the matrix that rotates the coordinate axis is R_{fixed}, the world coordinates (X, Y, Z) are

$$\begin{bmatrix} X \\ Y \\ Z \end{bmatrix} = R_{\text{fixed}} \begin{bmatrix} X_{\text{fixed}} \\ Y_{\text{fixed}} \\ Z_{\text{fixed}} \end{bmatrix} + \begin{bmatrix} F_x^{\text{fixed}} \\ F_y^{\text{fixed}} \\ F_z^{\text{fixed}} \end{bmatrix} \tag{9}$$

$$R_{\text{fixed}} = \begin{bmatrix} 1 & 0 & 0 \\ 0 & 0 & -1 \\ 0 & -1 & 0 \end{bmatrix}, \tag{10}$$

To obtain the relational expression for the fixed camera, this is modeled using homography as

$$\begin{bmatrix} X_{\text{fixed}} \\ Y_{\text{fixed}} \\ Z_{\text{fixed}} \\ 1 \end{bmatrix} = \begin{bmatrix} 1 & 0 & 0 & -F_x^{\text{fixed}} \\ 0 & 0 & -1 & F_z^{\text{fixed}} \\ 0 & -1 & 0 & F_y^{\text{fixed}} \\ 0 & 0 & 0 & 1 \end{bmatrix} \begin{bmatrix} X \\ Y \\ Z \\ 1 \end{bmatrix} \tag{11}$$

Assuming that $(F_x^{\text{fixed}}, F_y^{\text{fixed}}, F_z^{\text{fixed}})$ is the origin, (6) and (11) are combined as follows:

$$s \begin{bmatrix} x_{\max,t} \\ y_{\max,t} \\ 1 \end{bmatrix} = K_{\text{fixed}} T_{pers}(1) \begin{bmatrix} 1 & 0 & 0 & 0 \\ 0 & 0 & -1 & 0 \\ 0 & -1 & 0 & 0 \\ 0 & 0 & 0 & 1 \end{bmatrix} \begin{bmatrix} X \\ Y \\ Z \\ 1 \end{bmatrix} \tag{12}$$

This is solved to obtain the equation of a straight line for the global coordinates.

$$-\frac{f_x^{\text{fixed}}}{c_x^{\text{fixed}} + x_{\max,t}} X = Y = -\frac{f_y^{\text{fixed}}}{c_y^{\text{fixed}} - y_{\max,t}} Z \tag{13}$$

As a result, we need to obtain the coordinates for the telecentric zoom tracking camera. The field of view, which is the position where the image is formed, is $(F_x^{\text{zoom}}, F_y^{\text{zoom}}, F_z^{\text{zoom}} - D_w)$ at a distance from the working distance D_w from the position of the camera. Substituting the next position into (13), the searching path of the telecentric zoom tracking camera can be obtained.

$$-\frac{f_x^{\text{fixed}}}{c_x^{\text{fixed}} + x_{\max,t}} F_x^{\text{zoom}} = F_y^{\text{zoom}}$$
$$= -\frac{f_y^{\text{fixed}}}{c_y^{\text{fixed}} - y_{\max,t}} \left(F_z^{\text{zoom}} - D_w\right) \tag{14}$$

E. LARVA-TRACKING METHOD BY CARTESIAN ROBOT

If a near-view telecentric zoom tracking camera successfully finds the eel larva through its search, it requires physical tracking for continuous observation. We should perform a physical tracking movement with a 3-axis Cartesian robot that can move in three directions using information obtained from the zoom camera images. We performed tracing in two ways. First, we recognized the position of the larva in the captured image, and the x and y directions were controlled so that the position was at the center of the camera. Second, we controlled the z-directional movement so that the focusing was continuously applied to the capture result of the eel larva.

1) EEL LARVA DETECTION

For tracking in the X and Y directions, we controlled the Cartesian robot by detecting the position of the eel larva caught in the image. In the telecentric zoom tracking camera, the image is condensed only in the field of view area at a certain distance, and the only object that the camera can capture is an eel. Therefore, we can form a contour for pixels having a particular color or higher, and the x-axis and y-axis were controlled based on the center of mass of the contour.

2) AUTO-FOCUSING BASED Z-AXIS TRACKING

Tracking the z-axis is very difficult because it is impossible to determine the perspective within a single camera image. However, owing to the characteristics of the telecentric lens of the zoom tracking camera, the focus of the image is blurred as the larva moves in the z-direction. Therefore, we performed z-directional tracking using an image-focusing algorithm.

In general, an image with sharper edges can be considered a well-focused image. Therefore, by obtaining the gradient of the image representing the edge and obtaining the value, information on the image's focus can be obtained. We calculated the focus value using the Laplacian gradient method. It is a second derivative-based method, and it can be calculated as the second derivative in the x and y directions for the image $I(x, y)$.

$$L(I) = \frac{\partial^2 I}{\partial x^2} + \frac{\partial^2 I}{\partial y^2} \tag{15}$$

If we calculate the variance for $L(I)$ as follows, we can obtain the image's focus value.

$$Var(L) = \sum_{M}^{m} \sum_{N}^{n} [L(m, n) - \text{mean}(L)]^2 \tag{16}$$

F. IMAGE-ANALYSIS METHOD FOR BREEDING MANAGEMENT

We can analyze the images obtained using a vision-based precision monitoring system to obtain information for breeding management. For images obtained from a far-field fixed high-resolution camera, we can periodically estimate the number of larvae and identify changes in the survival rate. Moreover, we determined the behavioral patterns of the larvae before and after feeding. In addition, when mortality with

a sudden drop in survival rate occurred, it was possible to analyze the cause. In a near-field telecentric zoom tracking camera image, we can analyze the size and length of the eel larva. It is also possible to analyze a larva's path in a water tank using tracking results. These results can be used to enhance the breeding of eel larvae.

1) POPULATION ESTIMATION

Using the foreground subtraction mentioned earlier for the initial larval scan, we can estimate the distribution status of the larvae. However, there is a difference between the measured values of larvae showing movement in the image and the actual number. This is because there are blind spots that the camera cannot capture, and the larvae overlap because of filming in one direction. Therefore, a conversion equation was obtained and applied by comparing the actual number of larvae to the estimated distribution. To find the conversion formula, we placed 0-500 fish in units of 20 and calculated N_t of formula (1). Because the corresponding value changed slightly each time, we averaged the value over 30 frames. Furthermore, we obtained the trend line and derived the conversion equation as a first-order polynomial. As a result, the estimated population EP according to the average N_t satisfies the following equation, and the value obtained is $a = 2.22$.

$$EP = a * \frac{1}{30} \sum_{t=1}^{30} N_t \tag{17}$$

2) SHAPE ANALYSIS OF EEL LARVA

Shape analysis of the larvae is essential for understanding its growth state. Monitoring the size of the body at regular intervals can determine the growth rate of the larvae. We quantitatively determined the shape using a telecentric lens mounted on a near-field zoom tracking camera. Because this lens has the perspective removed, the proportion of the pixel value to the actual value of the length or area is always constant. Therefore, by using a calibration sheet, the scale ratio values s_x and s_y can be obtained, as shown in Fig. 8. The length of one side of each box of the calibration sheet was 1 mm. As a result, the ratio of the actual length to the pixel is $s_x = 0.00937$ and $s_y = 0.00947$. Subsequently, we can calculate the actual length and area from the pixel values of the larva's length and area in the images.

3) MOVEMENT ANALYSIS IN THE WATER TANK

The movement of the larva can be monitored and stored using a near-field telecentric zoom tracking camera. This is a crucial indicator of larval activity. The movement path coincides with the movement path of the 3-axis Cartesian robot that moves when tracking and observing the larva. The target position of the robot was recorded using shooting images. The target position represents the absolute value from the initial position of the robot, which can be converted into millimeters.
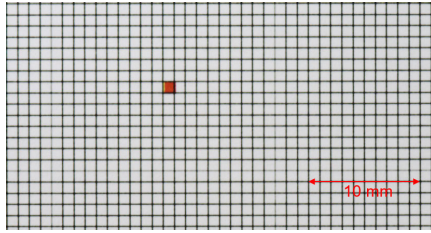
FIGURE 8. Telecentric zoom tracking camera calibration image (1 mm per side of the square).
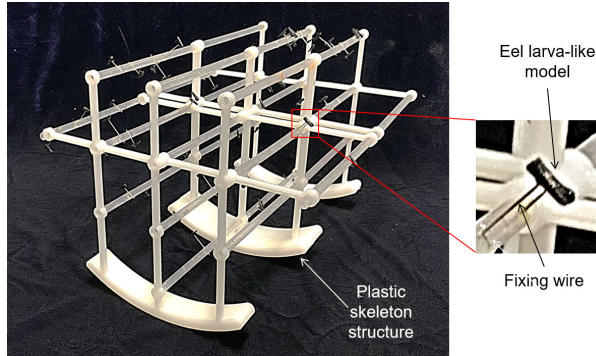

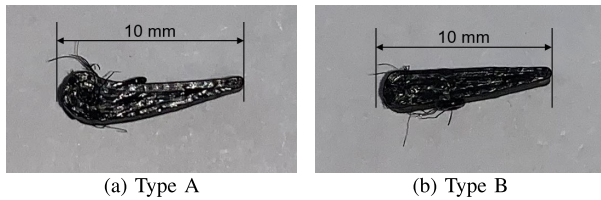**FIGURE 9.** Eel larva models with skeleton structure to emulate the eel larvae's position.

(a) Type A   (b) Type B

FIGURE 10. Image of eel larvae-like plastic models.

III. EXPERIMENT WITH EEL LARVA MODELS

For the quantitative evaluation of the shooting technique, we constructed an experiment where we randomly placed the eel larva models inside a water tank. Through this, we verified whether our fusion algorithm could successfully find tiny eel larvae by searching for a dense area.

A. 3D PLASTIC EEL LARVA MODEL STRUCTURE

We 3D-printed and assembled the plastic skeleton structure shown in Fig. 9, which were placed in the water tank. Then, two differently shaped larva-like models were randomly placed, as shown in Fig. 10. Twelve straight rods were attached to the structure, and we randomly arranged the larvae models among the four angles and two distances to the rods. We know the position values for all larva models because we accurately measured the positions of the rods and controlled the larva model's attachment. We created a model in which 50 larvae were evenly spaced in the water tank and tested the fusion-based tiny object imaging method. Table 1 shows the layout of the 50 eel larva models. The actual position of the eel larva model is as follows:

$$(x_{\text{actual}}, y_{\text{actual}}, z_{\text{actual}})$$
$$= (x_{\text{rod}} + l\cos(\theta), y_{\text{rod}}, z_{\text{rod}} + l\sin(\theta)). \quad (18)$$

TABLE 1. Layout of plastic eel larva models.

Larva Model #	Type	Rod Position (x, y, z) (mm)	Angle θ $(°)$	Distance l (mm)
# 1	A	$(-120, -10, 0)$	225	20
# 2	B	$(-120, -40, 0)$	45	20
# 3	B	$(-120, -100, 0)$	135	10
# 4	A	$(-120, -250, 0)$	135	20
# 5	A	$(-120, -260, 0)$	315	20
# 6	A	$(-60, -40, -60)$	135	10
# 7	A	$(-60, -80, -60)$	225	20
# 8	B	$(-60, -220, -60)$	45	10
# 9	A	$(-60, -280, -60)$	315	10
# 10	B	$(-60, -20, 0)$	225	20
# 11	B	$(-60, -30, 0)$	135	20
# 12	B	$(-60, -40, 0)$	315	10
# 13	A	$(-60, -130, 0)$	45	20
# 14	B	$(-60, -140, 0)$	45	10
# 15	B	$(-60, -30, 60)$	135	10
# 16	A	$(-60, -50, 60)$	315	10
# 17	A	$(-60, -80, 60)$	315	20
# 18	B	$(-60, -90, 60)$	225	10
# 19	B	$(-60, -100, 60)$	45	20
# 20	B	$(-60, -100, 60)$	225	20
# 21	A	$(0, -80, -120)$	135	20
# 22	A	$(0, -150, -120)$	45	20
# 23	B	$(0, -170, -120)$	315	10
# 24	A	$(0, -270, -120)$	225	10
# 25	A	$(0, -40, -60)$	225	10
# 26	A	$(0, -90, -60)$	135	20
# 27	B	$(0, -60, 0)$	225	20
# 28	A	$(0, -150, 0)$	45	10
# 29	B	$(0, -270, 0)$	45	20
# 30	A	$(0, -190, 60)$	45	20
# 31	B	$(0, -220, 60)$	45	10
# 32	B	$(0, -230, 60)$	135	10
# 33	A	$(0, -260, 60)$	225	10
# 34	A	$(0, -260, 60)$	315	20
# 35	A	$(0, -270, 60)$	225	20
# 36	B	$(0, -270, 60)$	315	10
# 37	A	$(60, -20, 0)$	315	10
# 38	B	$(60, -120, 0)$	45	20
# 39	A	$(60, -140, 0)$	45	10
# 40	B	$(60, -150, 0)$	135	20
# 41	A	$(60, -200, 0)$	135	10
# 42	B	$(60, -220, 0)$	225	10
# 43	B	$(60, -80, 60)$	225	10
# 44	A	$(60, -120, 60)$	225	20
# 45	B	$(60, -190, 60)$	135	20
# 46	A	$(60, -200, 60)$	135	10
# 47	A	$(60, -210, 60)$	45	20
# 48	B	$(60, -220, 60)$	315	10
# 49	B	$(60, -250, 60)$	45	10
# 50	A	$(120, -70, 0)$	45	10

B. COLLABORATIVE VISION-BASED SEARCH RESULT IN THE MODEL STRUCTURE

We fixed the larvae models inside the water tank and performed vision-based precision monitoring. Our fusion algorithm first obtains images from a far-view fixed high-resolution camera and recognizes larvae. However, because larva models do not move, it is not easy to recognize
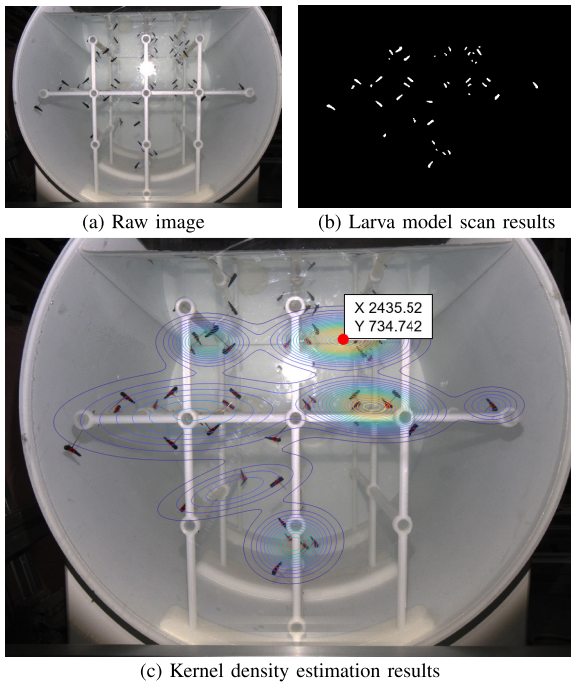
(a) Raw image

(b) Larva model scan results

X 2435.52
Y 734.742

(c) Kernel density estimation results

FIGURE 11. Larva model scan and kernel density estimation results.
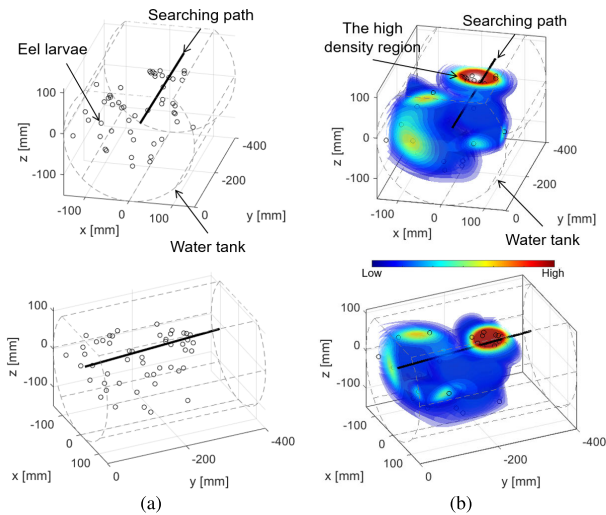

(a)

(b)

FIGURE 12. (a) Larva model positions and (b) 3D kernel density estimation result with the calculated searching path.

the models using the proposed foreground subtraction algorithm. Therefore, we detected the larvae models using a threshold using color. Subsequently, we applied kernel density estimation to find the coordinates with the highest density of larvae in the image. As a result, as shown in Fig. 11, we detected the larvae models and determined the highest density position.

When the positions of all the larva models in the tank are confirmed, we can obtain 3D density information for the larvae models inside the tank through 3D kernel density estimation. We calculated the searching path for the maximum density points of the larval models obtained using (14). In addition, we confirmed whether the fusion method that moves the zoom camera to the path is close to the
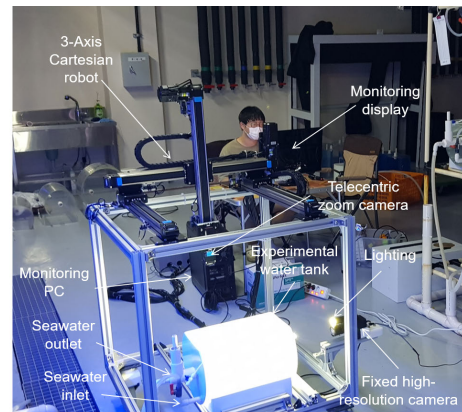

(a) Trajectory of telecentric zoom tracking camera

(b) Eel larva model # 44

(c) Eel larva model # 40

(d) Eel larva model # 45

(e) Eel larva model # 46

(f) Eel larva model # 42

FIGURE 13. Telecentric zoom tracking camera's underwater shooting result moving along the searching path.

FIGURE 14. Scene of the experiment with the actual eel larvae.

high-density point of the larvae models. As a result, Fig. 12 shows that the searching path passed from the model to the actual high-density area.

Next, the telecentric zoom tracking camera was moved along the path to the shoot. Fig. 13 shows the actual moving path of the zoom tracking camera and the photographs. The zoom camera was able to photograph five larval models while moving along the search path. Table 2 shows the actual position of the five photographed larva models and the position estimated to convert the moving coordinates of the Cartesian robot model. The root mean square error of position x is
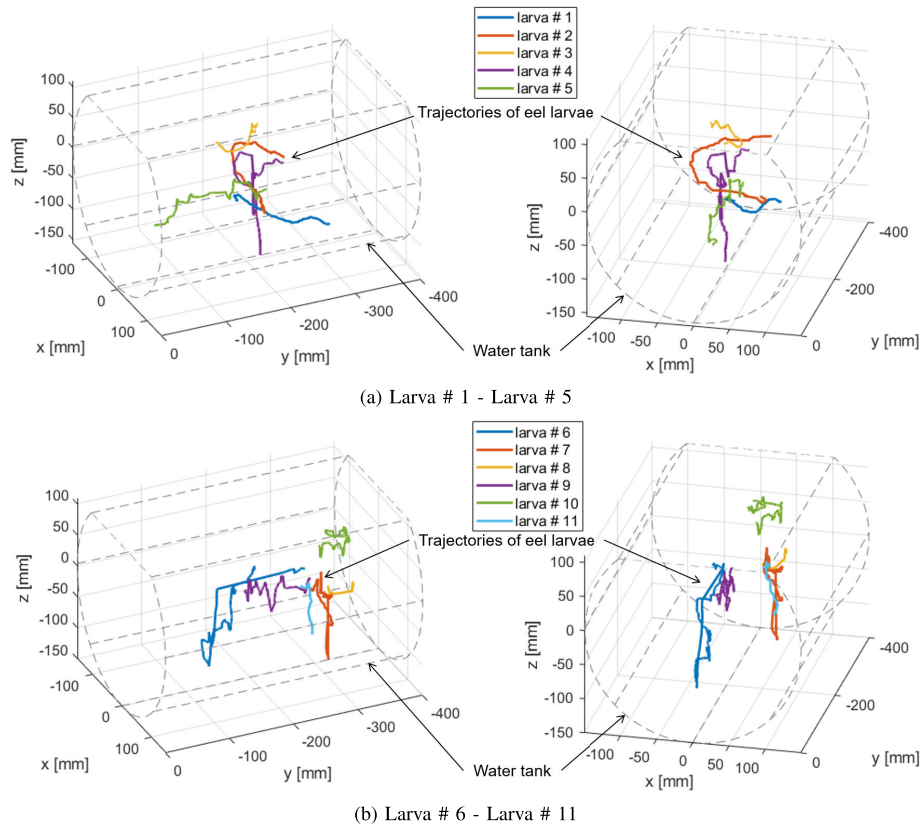
(a) Larva # 1 - Larva # 5

(b) Larva # 6 - Larva # 11

FIGURE 15. Obtained trajectories of eel larvae in the water tank.

TABLE 2. Estimated position of the telecentric zoom tracking camera's shooting result.

Larva Model #	Actual Position (x, y, z) (mm)	Estimated Position (x, y, z) (mm)
# 40	$(45.86, -150, 14.14)$	$(46.94, -151.95, 13.28)$
# 42	$(52.93, -220, -7.07)$	$(53.54, -222.56, -5.09)$
# 44	$(45.86, -120, 45.86)$	$(46.8, -119.55, 49.00)$
# 45	$(45.86, -190, 74.14)$	$(42.93, -188.40, 73.75)$
# 46	$(52.93, -200, 67.07)$	$(52.51, -200.28, 61.88)$

1.50 mm, that of position y is 1.62 mm and that of position z is 2.89 mm.

IV. EXPERIMENT WITH THE ACTUAL EEL LARVAE

A. EXPERIMENT SETTING

To evaluate the proposed method, we performed an experiment by placing live eel larvae into an experimental water tank, as shown in Fig. 14. We sufficiently prepared eel larvae, and images from 0 to 500 were taken in units of 20 to verify the population analysis. We photographed the telecentric zoom tracking camera image in a tank environment with 300 larvae. We repeatedly searched for eel larvae, and as a result, we obtained meaningful images of 11 eel larvae. In the case of zoom camera tracking, when a single larva is in the field of view, it is automatically tracked in the x and y directions, and tracking in the z direction is performed manually based on focusing.
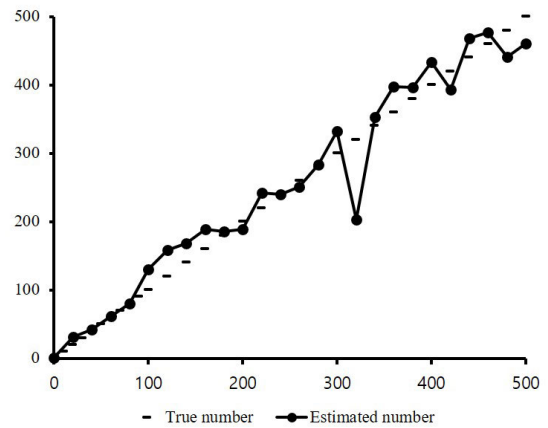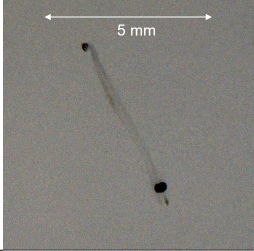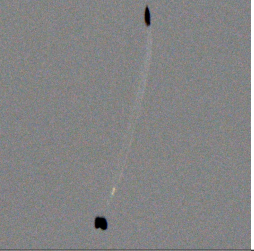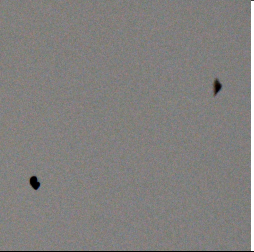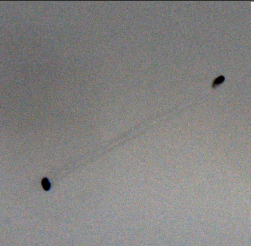

FIGURE 16. Population estimation result of eel larvae.

B. LARVAE POPULATION ESTIMATION

We estimated the population by placing eel larvae in the tank in increments of 20 from 0 to 500. Fig. 16 shows the true number of eel larvae according to the value of *EP*. The graph shows a meaningful trend in our estimation method, where the error from the true number was approximately 6.0%. As a result, we confirmed that the analysis results could later determine the approximate number of eel larvae in the water tank.

However, the sharp decrease in 320 larvae appears to be an error due to external factors. For example, there are cases in

TABLE 3. Length estimation results of telecentric zoom tracking camera images (Larva # 1 - # 11).

Larva #	Telecentric zoom camera image	body length (mm)	Larva #	Telecentric zoom camera image	body length (mm)	Larva #	Telecentric zoom camera image	body length (mm)
# 1		5.73	# 2		7.10	# 3		6.73
# 4		7.10	# 5		6.84	# 6		6.60
# 7		6.99	# 8		6.10	# 9		6.00
# 10		6.94	# 11		6.88			

which the background is shaken owing to vibration during the process of placing the larvae or temporary changes in external lighting. Moreover, such an error can occur even when the larvae are excessively clustered. The above cases can be solved by shooting after sufficient time has elapsed until the movement of the water tank is stable and controlling the surrounding brightness equally with a blackout curtain.

C. MOVEMENT ANALYSIS IN THE WATER TANK

As shown in Fig. 15, we determined the paths of the 11 larvae. The trajectories visualized the path of a 3-axis Cartesian robot in millimeters, and the data were synchronized with the video of the swimming activity of the eel larva. In the future, we can use the video to understand a single eel larva's path as it swims.

Next, we analyzed the images of eel larvae to determine the average length. The values calibrated in the method, $s_x = 0.00937$ and $s_y = 0.00947$, were obtained by converting the pixels of the image to the actual length. Fig. 17 shows
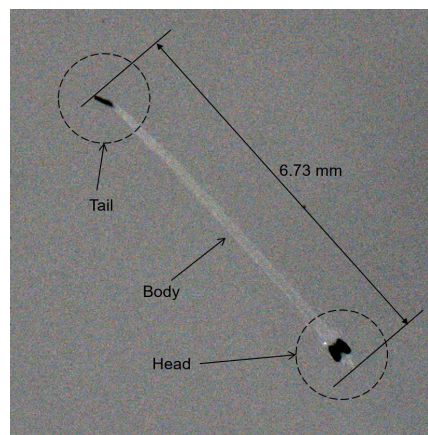

FIGURE 17. Analysis result of the telecentric zoom camera image (larva # 3).

the analysis results of larva # 3. We can observe the head, body, and tail of the eel larva and measured the length. As a result, we obtained images and lengths of each of the

11 larvae, as shown in Table 3. Furthermore, in this experiment, the average length of eel larvae was 6.64 mm.

V. CONCLUSION

This study proposes a system that can observe the actual eel larvae in a tank using two different cameras: a fixed high-resolution camera can observe the entire tank, and a telecentric zoom camera is attached to a 3-axis Cartesian robot that can move to enable tracking and imaging of eels from above the tank. We created plastic models that resemble eel larvae, verified the imaging algorithm in a water tank, and then successfully observed the actual eel larvae. In addition, we obtained objective information for eel larval breeding based on the two types of videos and robot path data. The number of individuals was estimated with fixed high-resolution camera images, the length of the eel larvae was obtained, and the motion was observed with telecentric zoom camera images. We can also obtain the movement path of eel larvae in a water tank by using the Cartesian robot's movement path. As a result, we verified that the proposed monitoring system effectively collected objective information for breeding small eel larvae.

Future work is expected to observe actual eel larvae over an extended period. In this study, we developed a system and performed observations of actual larvae. However, monitoring must be performed several times during a certain period. We will observe changes over a long period using our monitoring system to determine the changes that eel larvae undergo as they grow after hatching. As the eel larvae grow, their movements will change, and we will study this change using our observation device.

REFERENCES

[1] J. S. Jaffe, "Underwater optical imaging: The past, the present, and the prospects," *IEEE J. Ocean. Eng.*, vol. 40, no. 3, pp. 683–700, Jul. 2015.

[2] K. Tsukamoto, S. Chow, T. Otake, H. Kurogi, N. Mochioka, M. J. Miller, J. Aoyama, S. Kimura, S. Watanabe, T. Yoshinaga, A. Shinoda, M. Kuroki, M. Oya, T. Watanabe, K. Hata, S. Ijiri, Y. Kazeto, K. Nomura, and H. Tanaka, "Oceanic spawning ecology of freshwater eels in the Western North Pacific," *Nature Commun.*, vol. 2, no. 1, p. 179, Sep. 2011.

[3] K. Tsukamoto, T. Otake, N. Mochioka, T.-W. Lee, H. Fricke, T. Inagaki, J. Aoyama, S. Ishikawa, S. Kimura, M. J. Miller, H. Hasumoto, M. Oya, and Y. Suzuki, "Seamounts, new moon and eel spawning: The search for the spawning site of the Japanese eel," *Environ. Biol. Fishes*, vol. 66, no. 3, pp. 221–229, Mar. 2003.

[4] H. Tanaka, "Progression in artificial seedling production of Japanese eel anguilla japonica," *Fisheries Sci.*, vol. 81, no. 1, pp. 11–19, Jan. 2015.

[5] P. Edwards, "Aquaculture environment interactions: Past, present and likely future trends," *Aquaculture*, vol. 447, pp. 2–14, Oct. 2015.

[6] M. Føre, K. Frank, T. Norton, E. Svendsen, J. A. Alfredsen, T. Dempster, H. Eguiraun, W. Watson, A. Stahl, L. M. Sunde, C. Schellewald, K. R. Skøien, M. O. Alver, and D. Berckmans, "Precision fish farming: A new framework to improve production in aquaculture," *Biosyst. Eng.*, vol. 173, pp. 176–193, Sep. 2018.

[7] F. D. Von Borstel Luna, E. de la Rosa Aguilar, J. S. Naranjo, and J. G. Jaguey, "Robotic system for automation of water quality monitoring and feeding in aquaculture shadehouse," *IEEE Trans. Syst., Man, Cybern. Syst.*, vol. 47, no. 7, pp. 1575–1589, Jul. 2017.

[8] Y. Atoum, S. Srivastava, and X. Liu, "Automatic feeding control for dense aquaculture fish tanks," *IEEE Signal Process. Lett.*, vol. 22, no. 8, pp. 1089–1093, Aug. 2015.

[9] S. B. Chandanapalli, "Design and deployment of Aqua monitoring system using wireless sensor networks and IAR-kick," *J. Aquaculture Res. Develop.*, vol. 5, no. 7, p. 283, 2014.

[10] M. Saberioon, A. Gholizadeh, P. Cisar, A. Pautsina, and J. Urban, "Application of machine vision systems in aquaculture with emphasis on fish: State-of-the-art and key issues," *Rev. Aquaculture*, vol. 9, no. 4, pp. 369–387, Dec. 2017.

[11] E. Fontaine, D. Lentink, S. Kranenbarg, U. K. Müller, J. L. Van Leeuwen, A. H. Barr, and J. W. Burdick, "Automated visual tracking for studying the ontogeny of zebrafish swimming," *J. Experim. Biol.*, vol. 211, no. 8, pp. 1305–1316, Apr. 2008.

[12] N. Speedie and R. Gerlai, "Alarm substance induced behavioral responses in zebrafish (Danio rerio)," *Behavioural Brain Res.*, vol. 188, no. 1, pp. 168–177, Mar. 2008.

[13] J. Delcourt, C. Becco, N. Vandewalle, and P. Poncin, "A video multitracking system for quantification of individual behavior in a large fish shoal: Advantages and limits," *Behav. Res. Methods.*, vol. 41, no. 1, pp. 228–235, Feb. 2009.

[14] R. Benvenutti, M. Marcon, M. Gallas-Lopes, A. J. de Mello, A. P. Herrmann, and A. Piato, "Swimming in the maze: An overview of maze apparatuses and protocols to assess zebrafish behavior," *Neurosci. Biobehav. Rev.*, vol. 127, pp. 761–778, Aug. 2021.

[15] M. D. O. Barreiros, F. G. Barbosa, D. D. O. Dantas, D. D. M. L. D. Santos, S. Ribeiro, G. C. D. O. Santos, and A. K. Barros, "Zebrafish automatic monitoring system for conditioning and behavioral analysis," *Sci. Rep.*, vol. 11, no. 1, p. 9330, Dec. 2021.

[16] J. Cachat, A. Stewart, E. Utterback, P. Hart, S. Gaikwad, K. Wong, E. Kyzar, N. Wu, and A. V. Kalueff, "Three-dimensional neurophenotyping of adult zebrafish behavior," *PLoS ONE*, vol. 6, no. 3, Mar. 2011, Art. no. e17597.

[17] X. Liu, Y. Yue, M. Shi, and Z.-M. Qian, "3-D video tracking of multiple fish in a water tank," *IEEE Access*, vol. 7, pp. 145049–145059, 2019.

[18] R. J. Egan, C. L. Bergner, P. C. Hart, J. M. Cachat, P. R. Canavello, M. F. Elegante, S. I. Elkhayat, B. K. Bartels, A. K. Tien, D. H. Tien, S. Mohnot, E. Beeson, E. Glasgow, H. Amri, Z. Zukowska, and A. V. Kalueff, "Understanding behavioral and physiological phenotypes of stress and anxiety in zebrafish," *Behavioural Brain Res.*, vol. 205, no. 1, pp. 38–44, Dec. 2009.

[19] H. Wei, D. Peng, X. Zhu, and D. Wu, "A target tracking algorithm for vision based sea cucumber capture," in *Proc. 2nd IEEE Int. Conf. Comput. Commun. (ICCC)*, Oct. 2016, pp. 401–404.

[20] L. Ge, G. Gao, and Z. Yang, "Study on underwater sea cucumber rapid locating based on morphological opening reconstruction and max-entropy threshold algorithm," *Int. J. Pattern Recognit. Artif. Intell.*, vol. 32, no. 7, Jul. 2018, Art. no. 1850022.

[21] X. Qiao, J. Bao, L. Zeng, J. Zou, and D. Li, "An automatic active contour method for sea cucumber segmentation in natural underwater environments," *Comput. Electron. Agricult.*, vol. 135, pp. 134–142, Apr. 2017.

[22] F. Peng, Z. Miao, F. Li, and Z. Li, "S-FPN: A shortcut feature pyramid network for sea cucumber detection in underwater images," *Expert Syst. Appl.*, vol. 182, Nov. 2021, Art. no. 115306.

[23] J. Li, C. Xu, L. Jiang, Y. Xiao, L. Deng, and Z. Han, "Detection and analysis of behavior trajectory for sea cucumbers based on deep learning," *IEEE Access*, vol. 8, pp. 18832–18840, 2020.

[24] E. Gahtan, "Visual prey capture in larval zebrafish is controlled by identified reticulospinal neurons downstream of the tectum," *J. Neurosci.*, vol. 25, no. 40, pp. 9294–9303, Oct. 2005.

[25] S. D. Pelkowski, M. Kapoor, H. A. Richendrfer, X. Wang, R. M. Colwill, and R. Creton, "A novel high-throughput imaging system for automated analyses of avoidance behavior in zebrafish larvae," *Behavioural Brain Res.*, vol. 223, no. 1, pp. 135–144, Sep. 2011.

[26] C. L. Cario, T. C. Farrell, C. Milanese, and E. A. Burton, "Automated measurement of zebrafish larval movement," *J. Physiol.*, vol. 589, no. 15, pp. 3703–3708, Aug. 2011.

[27] P. R. Martineau and P. Mourrain, "Tracking zebrafish larvae in group–status and perspectives," *Methods*, vol. 62, no. 3, pp. 292–303, 2013.

[28] X. Wang, E. Cheng, I. S. Burnett, Y. Huang, and D. Wlodkowic, "Automatic multiple zebrafish larvae tracking in unconstrained microscopic video conditions," *Sci. Rep.*, vol. 7, no. 1, p. 17596, Dec. 2017.

[29] C.-Y. Chen and C.-M. Cheng, "Microfluidics expands the zebrafish potentials in pharmaceutically relevant screening," *Adv. Healthcare Mater.*, vol. 3, no. 6, pp. 940–945, Jun. 2014.

[30] K. Zhang, H. Zhang, H. Zhou, D. Crookes, L. Li, Y. Shao, and D. Liu, "Zebrafish embryo vessel segmentation using a novel dual ResUNet model," *Comput. Intell. Neurosci.*, vol. 2019, Feb. 2019, Art. no. 8214975.

[31] M. Cui, L. Su, P. Zhang, H. Zhang, H. Wei, Z. Zhang, and X. Zhang, "Zebrafish larva heart localization using a video magnification algorithm," in *Proc. IEEE Int. Conf. Mechatronics Autom. (ICMA)*, Oct. 2020, pp. 1071–1076.

[32] F. L. Lewis, D. M. Dawson, and C. T. Abdallah, *Robot Manipulator Control: Theory and Practice*. Boca Raton, FL, USA: CRC Press, 2003.

[33] M. Watanabe and S. K. Nayar, "Telecentric optics for focus analysis," *IEEE Trans. Pattern Anal. Mach. Intell.*, vol. 19, no. 12, pp. 1360–1365, Dec. 1997.

[34] N. Bouguila, "Finite general Gaussian mixture modeling and application to image and video foreground segmentation," *J. Electron. Imag.*, vol. 17, no. 1, Jan. 2008, Art. no. 013005.

[35] T. Duong, "KS: Kernel density estimation and kernel discriminant analysis for multivariate data in R," *J. Stat. Softw.*, vol. 21, no. 7, pp. 1–16, 2007.

JUHWAN KIM (Member, IEEE) received the B.E. degree in electrical engineering from the Pohang University of Science and Technology (POSTECH), Pohang-si, Republic of Korea, in 2015, where he is currently pursuing the Ph.D. degree with the Department of Convergence IT Engineering. He is a member of the Hazardous and Extreme Environment Robotics (HERO) Laboratory, POSTECH. His research interests include aquaculture engineering, underwater robotics, and multi-agent underwater manipulation.
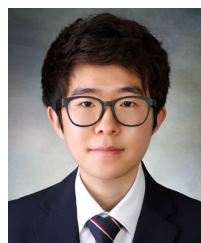
SEOKYONG SONG received the B.E. degree in creative IT engineering from the Pohang University of Science and Technology (POSTECH), Pohang-si, Republic of Korea, where he is currently pursuing the Ph.D. degree with the Department of Convergence IT Engineering. His research interests include underwater robotics, control, and manipulation systems.

TAESIK KIM received the B.E. degree in mechanical engineering from the Ulsan National Institute of Science and Technology (UNIST), Ulsan, Republic of Korea. He is currently pursuing the Ph.D. degree with the Department of Convergence IT Engineering, Pohang University of Science and Technology (POSTECH), Pohang-si, Republic of Korea. His research interests include underwater robotics, control, and manipulation systems.

YOUNG-WOON SONG received the B.E. degree in creative IT engineering from the Pohang University of Science and Technology (POSTECH), Pohang-si, Republic of Korea. He is currently pursuing the Ph.D. degree with the Department of Convergence IT Engineering. His research interests include autonomous underwater vehicles and field robotics.

SHIN-KWON KIM received the B.S. degree in marine production from Jeju National University, Jeju-si, Republic of Korea, in 1999, and the M.S. and Ph.D. degrees from the Tokyo University of Marine Science and Technology, Tokyo, Japan, in 2002 and 2005, respectively. He has been a Researcher with the National Research Institute of Aquaculture, Japan Fisheries Research Agency, from 2005 to 2009. Since 2009, he has been working with the Division of Aquaculture Science, National Institute of Fisheries Science, Busan, Republic of Korea.

BAE-IK LEE received the B.S. degree from the Department of Aquaculture, Pukyong National University, Busan, Republic of Korea, in 1985, and the M.S. and Ph.D. degrees from the Tokyo University of Marine Science and Technology, Tokyo, Japan, in 1988 and 1994, respectively. Since 1994, he has been working with the Division of Aquaculture Science, National Institute of Fisheries Science, Busan.

YONGWOON RYU received the B.S. degree in marine production and the M.S. degree in marine biology from Jeju National University, Jeju-si, Republic of Korea, in 2006 and 2008, respectively, and the Ph.D. degree from the Department of Fisheries Science, Hokkaido University, Hokkaido, Japan, in 2013. From 2012 to 2018, he worked as an Assistant Professor at the Ehime University, Ehime, Japan. Since 2019, he has been working with the Division of Aquaculture Science, National Institute of Fisheries Science, Busan, Republic of Korea.

SON-CHEOL YU (Member, IEEE) received the M.E. and Ph.D. degrees from the Department of Ocean and Environmental Engineering, The University of Tokyo, in 2000 and 2003, respectively.

He was a Researcher of mechanical engineering with the University of Hawai'i, from 2004 to 2007, and an Assistant Professor of mechanical engineering with Pusan National University, from 2008 to 2009. He is currently an Associate Professor with the Division of Advanced Nuclear Engineering, Departments of Convergence IT Engineering and Electrical Engineering, Pohang University of Science and Technology (POSTECH), Republic of Korea. He is also the Director of the Hazardous and Extreme Environment Robotics (HERO) Laboratory, the IEEE Ocean Engineering Society Korea Chapter, and the Gyeongbuk Sea Grant Center. His research interests include autonomous underwater vehicles, underwater sensing, and multi-agent-based robotics.

• • •